Newtonian Drop Impact with a Solid Surface

Brian L. Scheller and Douglas W. Bousfield
Dept. of Chemical Engineering, University of Maine, Orono, ME 04469

The spreading of Newtonian liquid drops after impact with a solid surface is reported for a range of liquid and surface properties, drop diameters, and impact velocities. Results for liquid viscosities up to 300 mPa·s are given. For a given drop diameter and velocity, a range of liquid viscosities result in splashing even for smooth surfaces. The maximum spread radius, made dimensionless with the drop radius, is correlated as $R^*_{max} = 0.61(Re^2Oh)^{0.166}$, *where Re and Oh are the Reynolds and Ohnesorge numbers, respectively. A model is proposed to account for inertial, viscous, and surface tension forces on the maximum spread radius. Good agreement is found between the model and experimental data from several sources.*

Introduction

Three phenomena of common interest in drop impact are the occurrence of splashing, the final spread radius, and the maximum spread radius. Splashing is important when fragmentation of the liquid or substrate can occur, such as in soil erosion, or when possible defects in a coating can occur. The final spread radius is of interest in a number of coating applications. The maximum spreading for a drop is relevant in applications such as ink-jet printing, spray coating, plasma spray coating, sputter coating in microelectronics production, and pesticide application; the actual drop coverage area is set by maximum spreading due to solidification, uptake of liquid into a porous substrate, or surface roughness holding liquid in the area of maximum spread.

Liquid-drop impact has received attention for a variety of applications. Mutchler and Larson (1971) and Lesser (1981) give the pressure distribution and jet cutting action in soil erosion. Engel (1955) reports the same effects and cavitation in the context of jet turbine wear. The heat transfer from a hot surface to an impacting liquid droplet is given by Wachters and Westerling (1966), Chandra and Avedisian (1991), and Shi et al. (1993). Bechtel et al. (1981), Oliver (1984), and Asai et al. (1993) studied the spreading of the liquid droplet to determine coverage area in ink-jet printing. Madejski (1976), Trapaga and Szekely (1991), Trapaga et al. (1992), and Watanabe et al. (1992) studied the process of deformation and solidification of molten droplets onto a cold substrate as in plasma spraying and spray forming. The dynamic contact angle of aqueous solutions on smooth wax surfaces was investigated by Elliott and Ford (1972). Some of these applications involve other phenomena besides the fluid mechanics of drop deformation and spreading.

Splashing occurs under certain conditions during drop impact. Worthington (1876, 1908) found that a mercury drop impacting a solid surface would leave a concentric ring of small droplets around a larger drop after recoil. Flash photography verified that fingers formed as the droplet expanded outward after impact; these fingers would break from the main drop to form small drops. Engel (1955), Levin and Hobbs (1971), Mutchler and Larson (1971), Stow and Stainer (1977), and Stow and Hadfield (1981) found splashing to occur for roughened surfaces but not smooth surfaces. The occurrence of splashing increases with surface roughness magnitude, impact velocity, drop size, and liquid surface tension. Stow and Stainer (1977) found that the number of drops formed by splashing to correlate to drop kinetic energy. After the initial impact, a shock front moves outward, diverting some of the downward liquid flow into radial flow as shown by the geometrical-acoustics model by Lesser (1981). Field et al. (1985) stated that jetting action occurs when the contact-edge speed falls below the compression-wave speed.

Engel (1955), Toda (1972), Stow and Hadfield (1981), Cheng (1977), Mingheng (1985), and Shi et al. (1993) give the maximum spreading of water drops. With the exception of Engel's work, all studied the effect of varying drop diameter and impact velocities. Asai et al. (1993) gave the maximum spreading for ink drops with viscosities from 2 to 7.5 mPa·s. Maximum spreading was determined by all investigators through use of a high-speed camera or electrical means. In all cases, the liquid viscosity was under 10 mPa-s, maximum

Present address of B. L. Scheller: Dept. of Paper and Printing Science, Western Michigan University, Kalamazoo, MI 49008.

spreading occurred in less than 10 μs, and maximum spreading was independent of surface roughness.

A number of theoretical models to predict maximum spreading radius are available in the literature, such as models by Madejski (1976), Cheng (1977), Chandra and Avedsian (1991), and Watanabe et al. (1992). Madejski's model included solidification, but this can be turned off. Engel (1955), Bechtel and Bogy (1981), Stow and Hadfield (1981), and Mingheng (1985) give theoretical analyses, but they do not provide easily used expressions or expressions that predict maximum spreading.

The final spreading radius for the drop is a function of the advancing or receding contact angle. If the drop is allowed to recoil to equilibrium, the final spreading will be set by the receding contact angle for the system, assuming there is no evaporation or absorption into the substrate. Schwartz and Silvestre (1972), Lopez et al. (1976), Greenspan (1978), Hocking and Rivers (1982), and Haley and Miksis (1991), among others, give the spreading behavior of liquid drops to its equilibrium state for advancing and receding contact angles.

Although the impact of water drops has been studied intensively in the literature, the work on viscous liquids is limited to under 10 mPa·s. We report here the final and maximum spreading of Newtonian drops with viscosities up to 300 mPa·s. The effects of viscosity, density, drop diameter, liquid surface tension, impact velocity, and liquid–solid interactions on the maximum spreading radius are characterized. For drops around 3.0 mm in diameter, the occurrence of splashing is found only for a specific range of viscosity, but not for low or high viscosities. From this work, a correlation between maximum spread radius and the dimensionless groups characterizing the liquid properties and drop velocity is presented. A phenomenological model is proposed to predict maximum spread radius as a function of the important variables.

Experimental Setup

Drops are formed with a pipette and accelerate under gravity to impact the surface as shown by Figure 1. A catch pan is used to divert drops while optical adjustments are made. A video recording system with microscope optics is used to capture the spreading and any splashing of the drop during impact. The optics are adjusted to focus around one meter from the microscope lens to prevent the lens from becoming dirty. A unique aspect of this experimental work is the use of a strobe to obtain high-speed information from standard video.

The test liquid is mixed following conditions needed for formation of a homogeneous mixture. For glycerin–water–

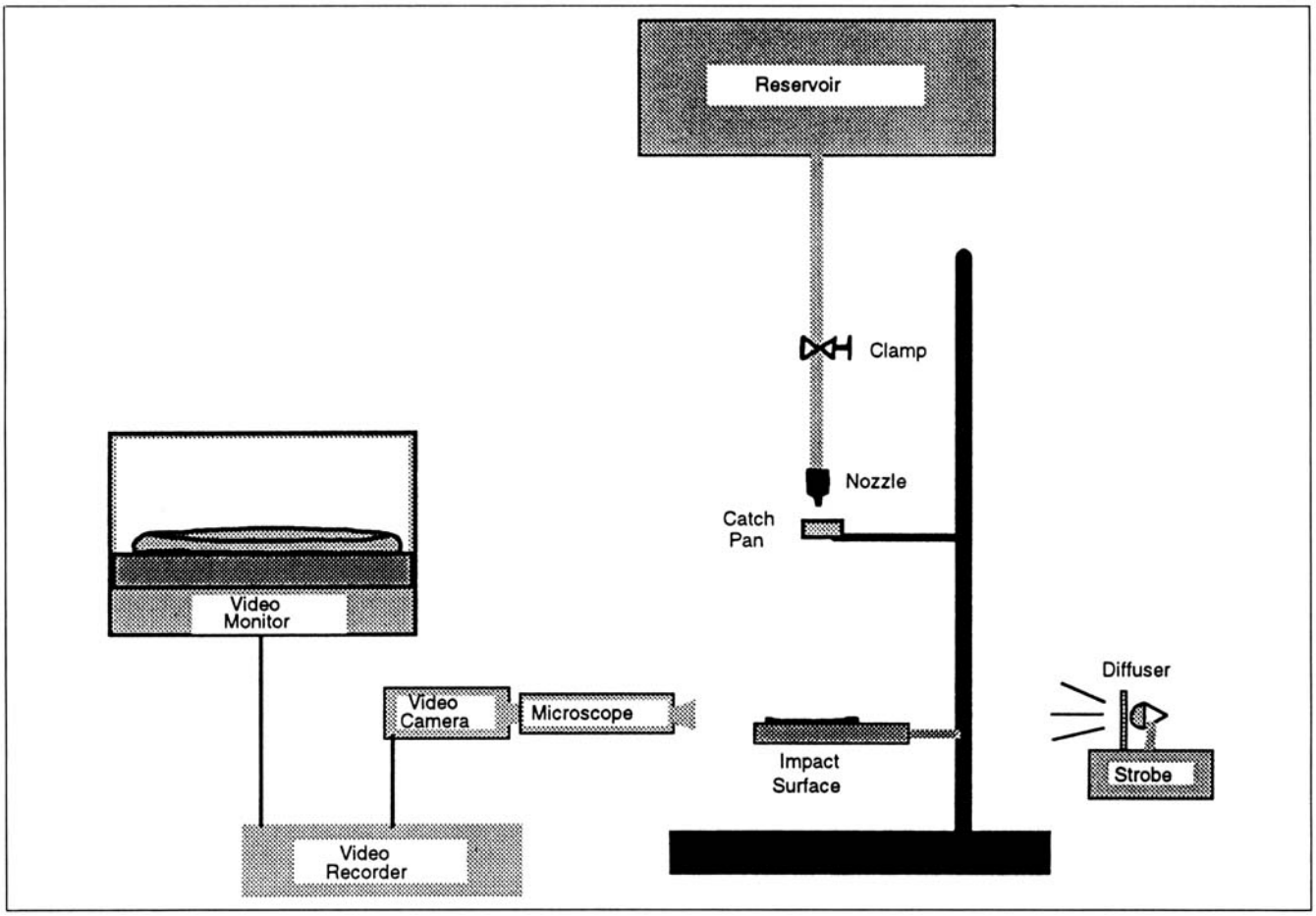

Figure 1. Experimental schematic for drop-impact experiments.
The strobe allowed high-speed information to be obtained on a standard video.

Table 1. Properties of Glycerin–Water Mixtures Used in Tests

Liquid Mixture	Viscosity (mPa·s)	Density ($\times 10^3$ kg/m^3)	Surface Tension (mN/m)
A	1.0	0.992	72.0
B	2.3	1.062	71.8
C	2.9	1.082	71.5
D	4.2	1.102	70.5
E	6.4	1.125	69.5
F	8.9	1.143	69.0
G	10.0	1.146	69.0
H	16.0	1.169	68.5
I	31.0	1.190	68.0
J	300.0	1.236	65.0

ethanol mixtures, the liquid is stirred and cooled to room temperature. The liquid viscosity is determined from the appropriate glass bulb capillary viscometer (Canon-Fenske) at ambient temperatures. Liquid density is determined by the weight of a volumetric flask. Surface tensions for the liquid mixtures were taken from literature values from Weast (1975) and Weast and Astle (1985) knowing the liquid temperature and back-calculating the component ratios from density and viscosity data. The surface tension, viscosity, and density of each mixture are given in Table 1.

Drops form at the end of the capillary at a steady flow rate driven by gravity. The drop diameter is a function of nozzle diameter, liquid density, and liquid surface tension, being a balance between gravitational and surface tension forces. There is some dependence of drop diameter on the time between drops, the shorter times giving a larger drop diameter. Fast drop formation, less than one second, gives approximately a 20% increase in weight and imparts an oscillation of the drop diameter. Therefore, flow rates are adjusted to give a consistent time of five seconds between drops. The drop diameter is measured by weighing ten drops and from images on the video screen. The drop weight varies by 5% in weight, which gives 2% variation in diameter. Different droplet diameters were formed for a given liquid by varying nozzle diameter from 0.8 to 4 mm.

Both polystyrene film and glass surfaces were used, with and without a hydrophobic surface treatment (Rain Away, Kafko Int. Ltd.). The average surface roughness was 0.005 and 0.09 μm for the glass and polystyrene surfaces, respectively, as characterized by a surface profilometer (Tencor Instruments). The surfaces were cleaned with ethanol and wiped with low lint paper between each impact to maintain a liquid contact angle within five degrees. The contact angles were measured from macroscopic views of the video, and were found to be repeatable and accurate within five degrees.

The drop velocity is determined by measuring the fall distance between strobe flashes just before impact. The velocity is calculated from the strobe frequency. The measured drop velocities show about 4% variation between drops, which must arise from small differences in flow rate or from vibrations. Drop velocities are measured within 2% and agree well with predicted velocities.

The drop impact behavior is recorded by allowing a single drop to fall past the catching pan and impact the surface. The microscope magnification is adjusted to give the maximum magnification possible and still capture the maximum spreading of the drop. The video recording rate is 60 frames/s, much too slow to catch the maximum spreading or splashing by itself. However, by use of the strobe at settings up to 420 Hz, equivalent recording rates of 420 frames/s can be reached; each video frame has seven images superimposed. Although the edge of the drop is difficult to resolve during spreading, the maximum spreading is obvious because the drop must stop before recoil. This method gives an effective time between images of 2 μs and allows the drop velocity to be determined for speeds up to 4.9 m/s. The seven images on the screen are not sharp, but the interface is not difficult to determine. Six to 20 impact tests are performed for each set of conditions. Maximum spread radius could be measured to within 0.3 mm with a standard deviation of less than 3%. The pixel resolution is not an issue because the interface is around 10 pixels in width from the background lighting.

With drop diameters greater than 3.6 mm, the drops are prone to periodic oscillation in shape during free fall. The oscillation is dampened by liquid viscosity. Diameter variation is small for drop heights over half a meter. The drop diameters along horizontal and vertical lines are captured on video before impact and the average diameter was taken as the actual drop diameter for scaling when needed.

The experiments were analyzed from video recordings to determine maximum spreading, final spreading, and the presence of splashing. The spreading radius was measured off the video screen and converted to actual spread radius. Length scales on the video screen were calibrated to actual length scales from images of a ruler held at the region of impact. The video camera viewed the impact from an angle a few degrees above the impact plane to allow viewing of the plane into the screen and to improve resolution. The drops were found to spread symmetrically, and maximum spread radius could be measured from the two-dimensional view. The drop recoil was not always symmetrical, which made the final spread radius less reproducible.

By recording identical conditions but separate impacts, the impact shape in time is pieced together as shown in Figure 2. Figure 2f shows how a torus often forms at the outer edge or rim for large spreading radius. The torus can form waves or fingers that can break to form small drops. In the case of small drops and high contact angles, the torus may even recoil strongly and small drops break off with inward velocities.

If splashing occurs in the early stages of impact, it is recorded on the video as a series of images showing the trajectory of the splash drops. Splashing is evident by observation of the drop after impact: small drops are obvious around the main drop. Determination of maximum spreading is difficult when splashing occurs. The speed of the video recordings does not reveal the splash mechanism, but captures the trajectory of the small drops.

Experimental Results

The final drop-spreading radius for glycerin–water mixtures on a polystyrene film is shown in Figure 3. The glycerin–water mixtures with the high viscosities correspond to high glycerin content. If surface energy of the plastic film is constant, the value of the final spreading should be set by the liquid surface tension and not be dependent on impact veloc-

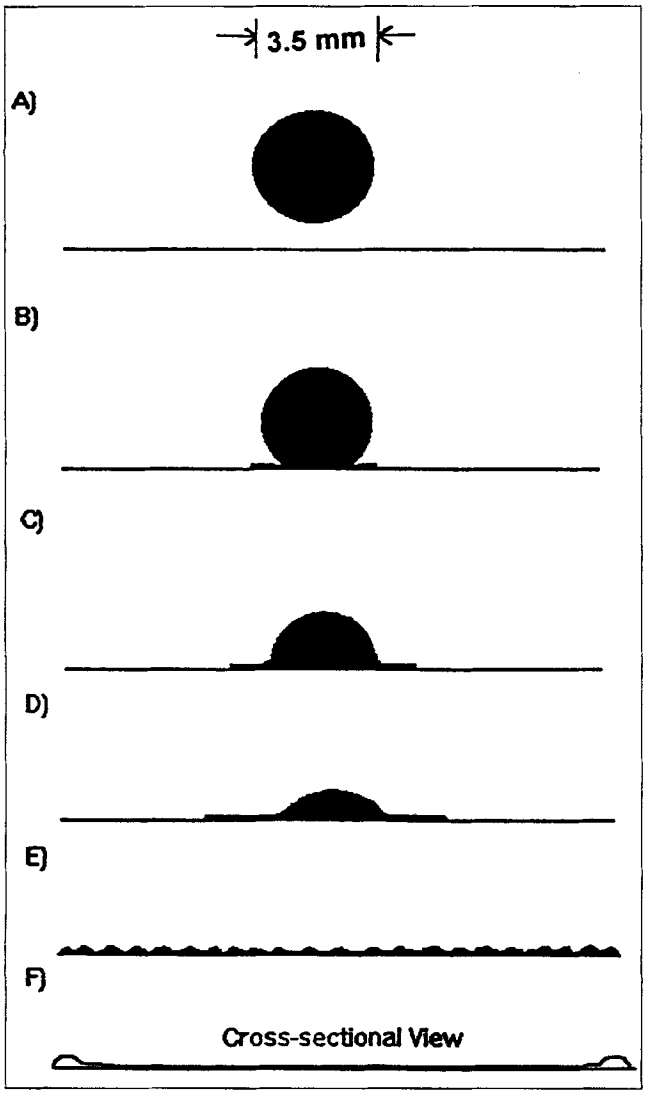

Figure 2. Impact shapes for a 3.5-mm water drop on a glass surface with (A) through (E) representing increasing time.

These shapes are taken from traces off the video screen. (F) is an expected cross-sectional view of shape (E).

ity. However, a dependence of the final radius on impact velocity does exist. This dependency on impact velocity must be a result of the nonsymmetric recoil or surface energies. The final spreading radius rapidly goes from a low value when set on the surface to some high values for all impact velocities. This is due to the difference between the advancing contact angle and receding contact angle, the lower spreading values set by advancing contact angle and the higher values set by receding contact angle.

Though smooth plastic and glass surfaces were used, splashing occurs in a viscosity "window" or a range of viscosities. For the polystyrene surface, splashing occurs for glycerin–water mixtures with viscosities from 2.5 to 7.0 mPa·s. This viscosity range is for impact velocities above 2.7 m/s and drop diameters over 3.5 mm. Water (1.0 mPa·s) and 10.0 mPa·s glycerin–water mixture did not show splashing even with velocities up to 3.8 m/s. The glycerin–water mixture on

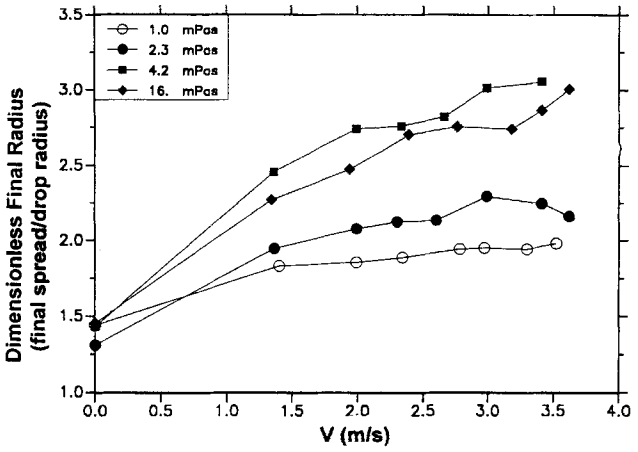

Figure 3. Final spread radius after drop recoil as a function of impact velocity for glycerin–water mixtures *A*, *B*, *D*, and *H* on polystyrene surfaces.

The final spread radius is made dimensionless with the initial drop radius.

polystyrene film has a static contact angle of 65°. For a hydrophobic glass surface, with a static contact angle of 70°, splashing occurs for viscosities from 5.7 to 25.0 mPa·s for impact velocities above 2.7 m/s. Splashing occurs in this viscosity range only for drops larger than 2.5 mm in diameter. Table 2 summarizes the splashing windows. Detailed data for every condition are in Scheller (1993).

Ethanol was added to the glycerin–water mixtures to reduce the surface tension to values of 40 to 45 mN/m for the same viscosities. For a tertiary mixture of water–glycerin–ethanol on a hydrophobic glass surface, splashing occurs for a viscosity range of 2.9 to 9.5 mPa·s, with drop diameter of 3.0 mm and impact velocities above 2.7 m/s. No splashing was found above or below these viscosities even with impact velocities up to 3.80 m/s.

This viscosity window for splashing has not been previously reported and is puzzling. The plastic surface, though it was rougher, has a smaller viscosity window for splashing. Increasing the viscosity should decrease the tendency for splashing because viscous dissipation of energy should be larger. The smooth glass surface with the high surface tension liquids had the largest viscosity range that produced splashing. The lower surface tension mixtures (when ethanol was added) decreased the splashing window. The viscosity window is largest for the higher surface tension liquids impacting a hydrophobic surface.

Table 2. Viscosity Ranges that Produce Splashing

Surface	Mixture	Viscosity (mPa·s)
Plastic	G-W	2.5–7.0
Glass	G-W	5.7–25
Glass	G-W-E	2.9–9.5

Note: All impact velocities are 2.7 m/s and all drops are around 3.0 mm diameter. G-W are glycerin–water mixtures. G-W-E are glycerin–water–ethanol mixtures.

The mechanism for splashing is not clear but may be related to the dynamic contact angle and the velocity of the contact line. A possible explanation for the splashing window deals with the speed of the dynamic contact line compared to the speed of the compression wave. The dependence of dynamic contact angle on viscosity and dynamic contact line velocity is given by an analysis from Jiang et al. (1979):

$$\frac{\cos\theta_s - \cos\theta_d}{\cos\theta_s + 1} = \tanh(4.96Ca^{0.702}) \qquad (1)$$

where θ_d and θ_s are the dynamic contact angle and static contact angle, respectively. The capillary number is given by $Ca = \mu V_c/\sigma$, where μ, θ, and V_c are the viscosity, liquid surface tension, and contact line velocity, respectively. Equation 1 shows that for a dynamic contact angle of 180° and a constant static contact angle, as the viscosity increases, the contact line velocity must decrease to keep the capillary number constant. The compression wave, which should have a constant velocity related to the speed of sound inside the drop, must be able to overtake the contact line and cause splashing. At higher viscosities, this compression wave must be attenuated by viscosity and become too weak to promote splashing. When surface tension is reduced, the static contact angle is reduced and the net effect of contact line velocity is not large compared to when just viscosity is changed.

Figure 4 shows the maximum spreading radius made dimensionless with drop radius, R^*_{max}, for various viscosity glycerin–water mixtures on polystyrene film for some of the liquids reported in Table 1. A complete listing of results is in Scheller (1993). A different dependence of maximum spreading on impact velocity for different liquid viscosities exists. The high viscosity liquids show small increase in maximum spreading with impact velocity, while water shows a higher degree of dependence on the impact velocity. This influence of velocity on maximum spreading is reported in the literature for water by Stow and Hadfield (1981) and others, but not for more viscous liquids.

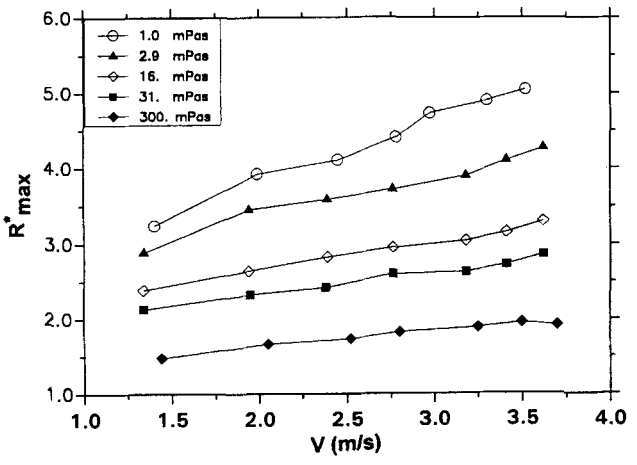

Figure 4. Maximum spread radius, R^*_{max}, as a function of impact velocity for glycerin–water mixtures *A*, *C*, *H*, *I*, and *J* on polystyrene film.

Higher viscosities result in smaller amounts of spreading and a smaller dependence on velocity.

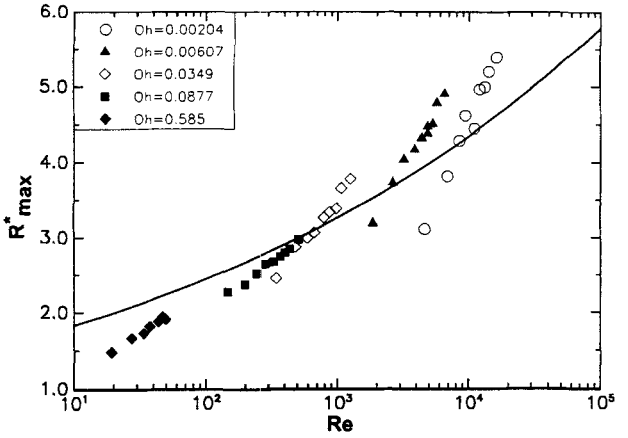

Figure 5. Maximum spread radius R^*_{max} for the glycerine–water mixtures plotted in Figure 4 as a function of drop Reynolds number.

Increasing Ohnesorge numbers represent increasing liquid viscosities. The line is Eq. 9.

Dimensional analysis gives four independent dimensionless groups to characterize drop impact. The ratio of liquid–solid surface energies and gravity are not expected to be important at significant velocities. Two remaining groups are the drop Reynolds number and the Ohnesorge number. The Reynolds and Ohnesorge number are given by

$$Re = \frac{\rho DV}{\mu}$$

$$Oh = \frac{\mu}{\sqrt{\rho D\sigma}}.$$

The Reynolds number characterizes the inertia to viscous forces; the Ohnesorge number contains information about liquid properties. Choosing the Ohnesorge number instead of the Weber or capillary number to characterize drop impact is arbitrary, but the Ohnesorge number is not a function of velocity and is only a function of the liquid properties. The Ohnesorge number is constant for every liquid and therefore resembles the familiar Prandtl and Schmidt numbers.

Figure 5 shows the dependence of maximum spreading radius R^*_{max}, on the Reynolds number for different Ohnesorge numbers for the same liquids as in Figure 4; increasing the Ohnesorge number corresponds to increasing viscosity liquids. This shows how the Ohnesorge number must be included in the determination of maximum spreading and represents different fluid properties. The change in slope and the shift of the line indicates a complex relationship between the parameters.

Figure 6 shows all the experimental results with the characterizing group, Re^2Oh. A regression with this group gives

$$R^*_{max} = 0.61(Re^2\,Oh)^{0.166}. \qquad (2)$$

This expression results in a correlation coefficient of 0.963 with the data. The maximum error in calculation of $ReOh$ is 9%, and the maximum error in dimensionless maximum

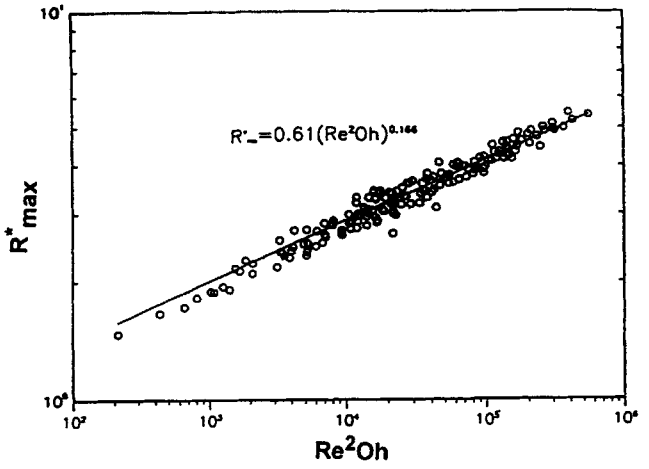

Figure 6. Experimental results for maximum spreading radius correlated against the dimensionless group $Re^2 Oh$.

The different viscosities all collapse into a line on this plot. The viscous results correspond to low values of $Re^2 Oh$. Small viscosities and high velocities correspond to large values of $Re^2 Oh$.

spreading radius is 5%. The characterizing group seems to correctly incorporate the dependence of maximum spreading on Reynolds and Ohnesorge numbers. The experimental results for the correlation encompass the following range of variables: liquid viscosity, 1–300 mPa·s; liquid surface tension, 40–73 mN/m; contact angles, 35–90 deg; drop diameters, 2.0–4.0 mm; and impact velocities, 1.30–4.90 m/s. The Reynolds and Ohnesorge numbers ranged from 19 to 16,400 and 0.0020 to 0.58, respectively. For some conditions of viscosity and impact velocities, the maximum spreading could not be determined due to liquid splashing. The liquid density was not changed on purpose but varies with glycerin content by 10%.

Figure 7 compares the preceding correlation to available literature results. Most of the literature data consist of low-

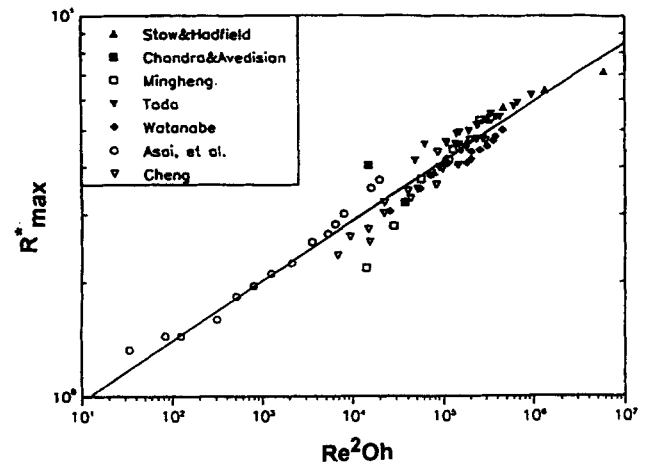

Figure 7. Experimental data of the literature vs. the regression line in Figure 6.

Many of the points below the line correspond to low-velocity results that may be influenced by contact angles or gravity.

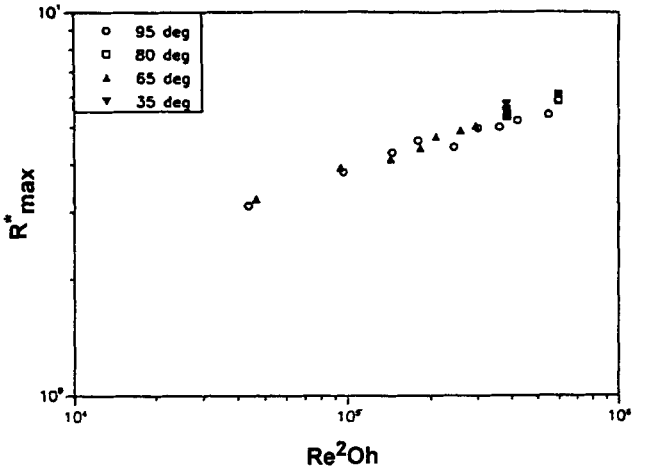

Figure 8. Influence of contact angle on maximum spreading radius.

The effect is less than 10%.

viscosity liquid-drop impact. The literature results give good fit to the master curve, especially considering the extreme conditions of Asai et al. (1993), where drop diameters are two orders of magnitude smaller and velocities are an order of magnitude larger than those presented here. The low-velocity literature result of Chandra and Avedisian (1991) and Mingheng (1985) lie off the regression line, but the low velocities result in Reynolds number is below the range of the correlation; the spreading for gentle impacts does not flatten the drop and is determined by the solid–liquid–vapor interfacial forces, not the viscous forces.

The static contact angle is found to have little effect on maximum spreading for drop Reynolds numbers over 10, as shown in Figure 8. Asai et al. (1993) found that even for ink-jet drop impact, the maximum spreading was independent of the surface for different grades of paper and plastic films. Stow and Hadfield (1985) found that the maximum spreading is independent of roughness. This indicates that the solid–liquid interaction plays a small role in maximum spreading for significant drop Reynolds numbers.

Squeeze Flow Model for Drop Impact

Drop impact is a complex event. The drop's downward momentum is converted to radial flow; surface tension and surface energies play an important role at low velocities; the pressure pulses are known to influence the spreading dynamics and splashing; and the drop oscillates at times during spreading. In addition, this is a transient free-surface problem with a moving contact line. A complete analysis of this problem would require finite-element techniques with inertial terms and a free surface. However, the results indicate that the maximum spreading is controlled by a simple inertia–viscosity–surface tension interplay. Even though shock waves and surface oscillations occur, the drop's kinetic energy must be dissipated by viscous flow. A phenomenological model of drop impact therefore is proposed here.

The geometry of the situation is simplified by assuming that the viscous damping is represented by the squeezing of a liquid cylinder that is twice the volume of the drop; twice the

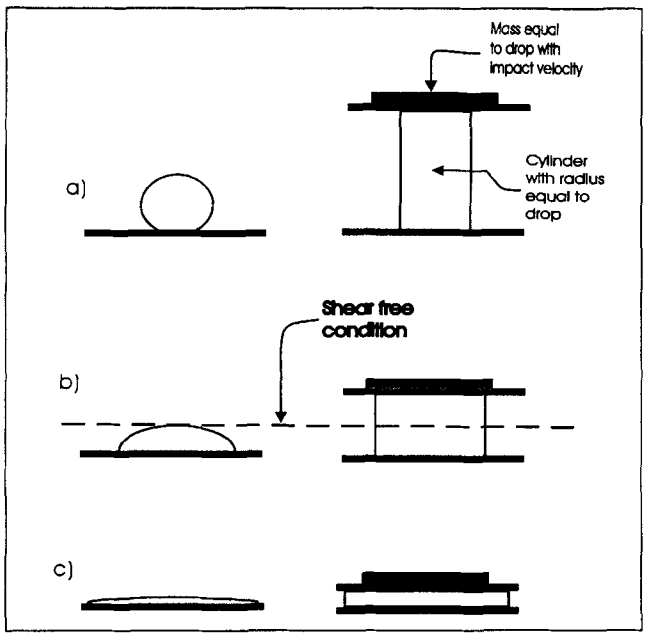

Figure 9. Squeeze flow model of droplet impact.

Drop spreading is represented by a cylinder of liquid on the righthand side of the figure slowing down the motion of a mass moving at the impact velocity. The initial radius of the cylinder equals the drop radius as shown in (a). The volume of the cylinder is twice the volume of the drop to represent the no-shear condition at the drop surface. The cylinder's radius increases in time as the mass slows down, as (b) and (c) illustrate.

volume is used to match the no shear condition of the drop's surface and the center line of the cylinder. The initial radius of the cylinder is set equal to the drop radius to scale the dissipation with the drop radius. Figure 9 illustrates the model. The inertia of the drop is represented by a body with a mass and velocity equal to the drop at the moment of impact: the velocity of this body must be decelerated in time by the squeezing of the cylinder between the two plates. The radius of the cylinder increases in time as the mass is decelerated. Surface tension forces are calculated from the curvature of the cylinder's surface. The cylinder's final radius is the maximum spread radius and depends on drop diameter, impact velocity, and the liquid properties such as density, viscosity, and surface tension. The model differs from past models in that the geometry is simple and inertia is included as a deceleration of a mass. The basic interaction between inertial, viscous, and surface tension forces should be captured by the model.

The downward velocity of the mass is described by Newton's law:

$$\frac{dU}{dt} = \frac{F_{tot}}{m_d} \tag{3}$$

where U is the downward velocity, F_{tot} is the total force acting on the mass, and m_d is the mass of the drop. From Lee et al. (1982), the viscous force F_{vis} is given by

$$F_{vis} = -\frac{3\pi\mu UR^4}{2H^3} - \frac{2\pi\mu UR^2}{H} \tag{4}$$

where R and H are the current radius and height. The negative sign is to cause the force to be positive for negative values of U. The first term is from the standard result for squeeze flow between two plates. The second term in Eq. 4 is the resistance from biaxial extension. Equation 4 does not include inertial effects and invokes the pseudo-steady-state approximation. The axial inertial terms are included approximately by the mass. The radial inertial terms will influence the dynamics of spreading. However, the radial velocities are zero before and after spreading and should not influence the maximum spreading.

The surface tension force must be estimated from the variables measured in the model. Though the viscous flow is calculated from a vertical cylinder, the drop surface is highly curved in the vertical direction. The capillary forces depend on the curvature of the drop's surface at the leading edge. The curvature in the vertical direction will scale with the height of the cylinder. The surface tension forces generate a capillary pressure or a pressure jump inside the cylinder. This pressure should be multiplied by the area of liquid in contact with the surfaces. The force from surface tension is estimated to be

$$F_{\text{surf}} = \sigma\left(\frac{1}{R_1} + \frac{1}{R_2}\right)\pi R^2 = \sigma\left(\frac{4}{H} + \frac{1}{R}\right)\pi R^2. \tag{5}$$

The first term $(4/H)$ accounts for the radius of curvature in the vertical direction; twice the liquid volume is assumed in the model and the curvature is half the cylinder height to produce the value of four. The second term in Eq. 5 accounts for the radius of curvature in the θ direction and is the radius of the cylinder.

Conservation of mass states that the cylinder radius and height are related as

$$R^2H = R_0^2H_0 \tag{6}$$

where R_0 and H_0 are the initial radius and height of the cylinder, respectively. The initial radius of the cylinder is taken to be the radius of the drop. The initial height of the cylinder is determined by setting the volume of the cylinder to twice the drop volume

$$H_0 = \frac{8R_0}{3}. \tag{7}$$

Setting the cylinder volume to be twice the volume of the drop is to match the no shear condition at the center line as pointed out in Figure 9. The mass in Figure 9 is taken to be equal to the mass of the drop $4\pi R^3\rho/3$, where ρ is the density of the liquid.

The radius is eliminated from the equations with Eq. 6. The forces are added ($F_{\text{tot}} = F_{\text{vis}} + F_{\text{surf}}$) and inserted into Eq. 3. The differential equation for H and U becomes

$$\frac{dU^*}{dt^*} = -\frac{81U^*}{256ReH^{*5}} - \frac{3U^*}{ReH^{*2}} + \frac{4}{Re^2Oh^2}\left(\frac{1.5}{H^{*2}} + \frac{1}{H^{*1/2}}\right). \tag{8}$$

The variables are made dimensionless as follows:

$$U^* = \frac{U}{V}$$

$$H^* = \frac{H}{H_0}$$

$$t^* = \frac{tV}{H_0}$$

where Re and Oh were defined earlier, V is the drop impact velocity, D is the drop diameter, and H_0 is the initial height of the cylinder given by Eq. 7. Equation 8 represents the base model proposed here. Besides the arguments imposed in setting up the model, there are no adjustable parameters.

The equation is solved by integrating Eq. 8. When the velocity is zero, the final thickness and the maximum spreading radius, R^*_{max}, are known. When no surface tension forces are included, an analytical result is possible. When only the first viscous term in Eq. 4 is used, the maximum spread radius is given by

$$R^*_{max} = (1 + 12.64Re)^{1/8}. \tag{9}$$

This expression gives a line through most of the data but has a slope that is too low, as shown by the line in Figure 5. In addition, this expression does not discriminate about different liquid properties. If both viscous terms are used, an implicit expression is obtained

$$R^*_{max} = [1 + 12.64Re + 6.31(1 - R^{*2}_{max})]^{1/8}. \tag{10}$$

This does move the model predictions toward the data at small values of the Reynolds number, but the changes are small. This change does not correct the overprediction of spreading by the model at low Reynolds numbers.

Figure 10 compares the base model results of Eq. 8 to the experimental results of the maximum spread radius: Eq. 8 is integrated numerically until the velocity of the top surface is zero. The radius of the cylinder at this point is taken as the spread radius. Given the choices for the cylinder's initial height and radius and the estimated curvature in the vertical direction, the model is predictive, with no adjusted parameters. At small drop spreading, the model overpredicts the experimental results, while at large drop spreading, the model underpredicts the final radius. A regression of the model results for the range of data gives

$$R^*_{max} = 1.0(Re^2\,Oh)^{0.123} \tag{11}$$

with correlation coefficient of 0.979. The dependence on Re^2Oh from the regression of the experimental results was given as 0.166. The model gives a lower slope than the experimental results, overpredicting at small spreading and underpredicting at large spreading.

In the case of large maximum spreading, the impact velocities are high and the liquid viscosity low. At these conditions, jetting of the liquid past the dynamic contact line is seen;

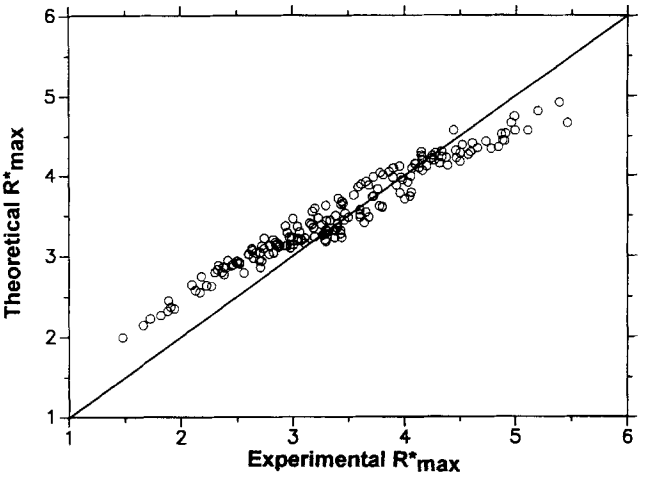

Figure 10. Comparison of model predictions with experimental results.

The model overpredicts spreading at high viscosities and low velocities, but underpredicts for low viscosities and high velocities. The 45° line is shown.

liquid is ejected over the contact line and falls downward onto the surface. This liquid undergoes extensional rather than shear flow and a corresponding reduction in viscous dissipation takes place. From an energy viewpoint, this would be free-spreading. With the model, liquid is spread without undergoing shear.

To account for the jetting action, a parameter is needed to account for the possibility that the velocity of the contact line could be smaller than the velocity of the cylinder's center. Figure 11 shows the contact line velocity, V_c, where the contact line is trailing the bulk fluid flow and the dynamic contact angle is approaching 180°. In the squeeze flow model, the viscous force, which is calculated from Eq. 4, should use R^* for the shear component and R^*_{bulk} for the biaxial extensional force component. The value of R^*_{bulk} is still calculated from Eq. 6, but R^* is increased in time linearly as

$$R^* = V_c^* t^* + 1 \tag{12}$$

where V_c^* is made dimensionless with V. Although V_c^* is dependent on the bulk radial velocity, for simplicity we assume it to be constant.

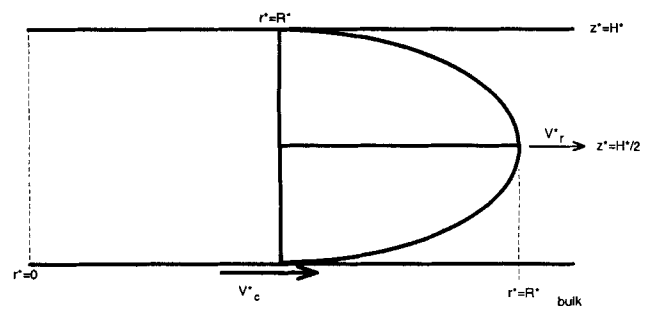

Figure 11. Edge of squeezing flow showing possible free spreading of the fluid at high radial velocities.

V_c^* is the contact line velocity and V_r^* is the velocity of the cylinder center.

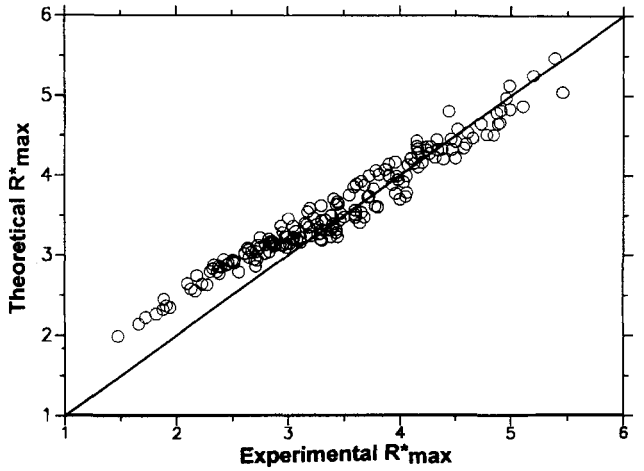

Figure 12. Comparison of model predictions with experimental results when free spreading is included in the model.

Improvement is obtained for large spreading results.

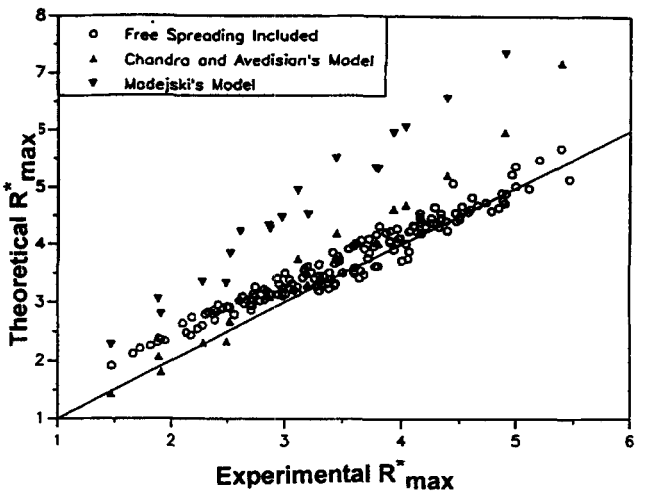

Figure 14. Comparison of current model predictions with other models reported in the literature.

The 45° line is shown. Earlier models predict the correct trends, but only in certain regions.

Now V_c^* becomes an input to account for spreading caused by the jetting mechanism. This value is used to adjust the model to fit to experimental results at high Reynolds number and is held constant for all fluids though this value should be a function of viscosity. V_c^* could be a value that can be obtained from dynamic contact angle experiments and Eq. 1. Figure 12 shows the comparison between the experimental and squeeze flow model results for dimensionless maximum spreading radius with the parameter $V_c^* = 1.4$. Regression of the model results gives the dependence on Re^2Oh as

$$R^*_{\max} = 0.91(Re^2\,Oh)^{0.133}. \qquad (13)$$

The parameter improves the prediction at larger dimensionless maximum spreading values, and overall gives a better match to the experimental results.

Figure 13 shows the dependence of the model with free spreading on Reynolds number for various Ohnesorge numbers. The data of Mingheng (1985) that fell below the correlation are the filled circles in Figure 13. The only parameter is the contact line velocity as described earlier. At low Reynolds numbers, each curve goes toward a value of one that corresponds to no spreading. However, this transition to a value of one occurs at different Reynolds numbers for different liquid properties. The model does describe data well and discriminates between the different liquid properties. Only for the two viscous liquid does the model overpredict spreading: this overprediction may be a result of the simplified geometry (a cylinder) to represent a low spreading result (a half sphere). Large spreading results do resemble a flat cylinder that is thin.

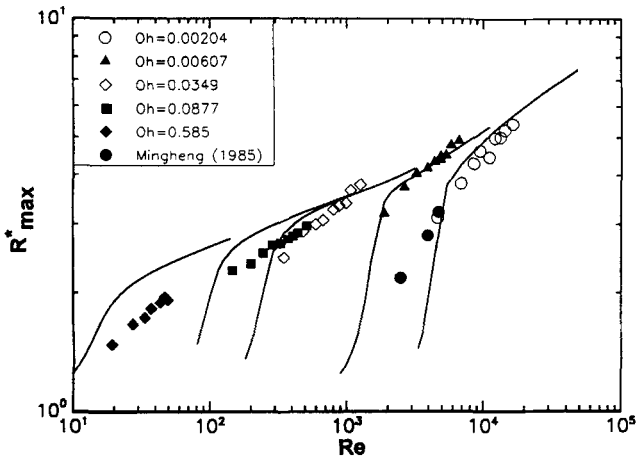

Figure 13. Free spread model predictions for various values of Ohnesorge number for the experimental data reported in Figure 4.

The filled circles are water data from Mingheng (1985).

Figure 14 compares the model to literature models for prediction of maximum spreading radius and the experimental regression curve. The model of Chandra and Avedisian (1991) is good at low maximum spreading, but overpredicts spreading at larger values. The predictions given for Chandra and Avedisian are assuming a dynamic contact angle of 180°. The predictions from Madejski (1976) are valid for Reynolds and Weber numbers greater than 100. However, the model was found to give a better fit at low maximum spreading conditions where this condition does not hold. The other energy conservation models either failed to give maximum spreading predictions or gave drastic overpredictions of the spreading because it ignores the effect of viscosity.

Table 3 compares the experimental and theoretical correlations from literature with the results given here; the other theoretical results are put in terms of Reynolds and Ohnesorge numbers. Figure 15 shows the correlations in Table 3 for comparison. Madejski's model matches the slope of the experimental data, but is shifted upward. Chandra and Avedisian's model gives a good fit at low spreading but overpredicts at higher spreading. The present model presented here overpredicts at low spreading and gives better fit at higher spreading when free spreading is included.

Table 3. Past Models in Terms of Reynolds and Ohnesorge Numbers

Experimenter	Prediction
Madejski (1976) (theoretical)	$\frac{3R_{max}^{*2}}{Re^2 Oh^2} + \frac{1}{Re}\left(\frac{R_{max}^*}{1.2941}\right)^5 = 1$
Cheng (1977)	$R_{max}^* = 0.816(Re^2 Oh^2)^{0.25}$
Chandra and Avedisian (1991) (theoretical)	$\frac{3}{2} Re Oh^2 R_{max}^{*4} + (1-\cos\theta)R_{max}^{*2} - \left(\frac{Re^2 Oh^2}{3} + 4\right) = 0$
Experimental results	$R_{max}^* = 0.61(Re^2 Oh)^{0.166}$
Base model	$R_{max}^* = 1.0(Re^2 Oh)^{0.123}$
Free spreading model ($V_c^* = 1.4$)	$R_{max}^* = 0.91(Re^2 Oh)^{0.133}$

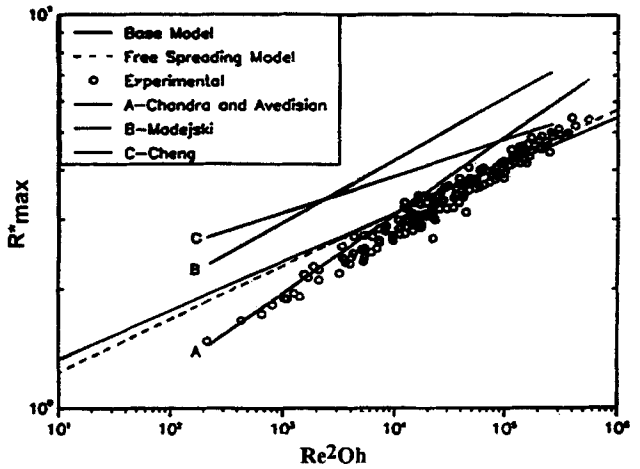

Figure 15. Comparison of various models with the current experimental results.

——, base model given by Eq. 8; – – –, free spread model.

Table 4 compares the average deviation of the maximum spreading radius from the theoretical models in Table 3 to the results available in the literature. Experiments from the literature are read down and the theoretical predictions read across. Experimental conditions from the literature include low surface tension liquids and small drops. The far right column gives the composite average deviation for all the literature experiments. The base and free-spreading model give the best overall prediction of results found in the literature.

The underprediction of the model at high Reynolds number is explained by the jetting of liquid from the drop, but the reason why the model overpredicts spreading at high viscosities is not clear. From an energy viewpoint, the drop is dissipating energy more rapidly than the squeeze flow between two disks. The mechanism for this higher dissipation could come from the thin liquid layers near the moving contact line. Biaxial extensional flow does not explain the results. The proposed equations and model should be used with caution, especially outside the range studied. A better understanding of contact line motion may explain the results.

Conclusions

The maximum spreading radius of Newtonian liquid drops during impact is correlated for a range of velocities and liquid viscosities. The correlation is based on Reynolds and Ohnesorge numbers and gives good fit to results available in the literature and the new viscous results. The Ohnesorge number is chosen as a second dimensionless group because it contains liquid properties and is independent of velocity.

A range of viscosities results in splashing, even with the smooth surfaces studied. The viscosity range for splashing increases with increasing drop size, drop velocity, liquid surface tension, and static contact angle.

The proposed model gives a good prediction of maximum spreading for results found in the literature and by present experiments, even for low surface tension fluids and microscopic drops. Including "free spreading" in the model improves predictions at high Reynolds numbers. The model discriminates between different liquids and describes data outside the range of the correlation. Regression of the model results gives a simple relationship between maximum spreading and Reynolds and Ohnesorge numbers.

Table 4. Comparison of Theoretical Models with Experimental Results*

	Toda (1972)	Cheng (1977)	Stow and Hadfield (1981)	Mingheng (1985)	Watanabe et al. (1982)	Asai et al. (1993)	Present Results	Average Deviation
Madejski (1976)	2.360	2.162	2.936	1.962	2.659	0.816	1.616	**2.073**
Cheng (1977)	1.264	0.342	0.988	0.971	0.554	0.563	0.936	**0.803**
Chandra (1991)	0.935	0.895	1.500	0.680	1.296	0.070	0.570	**0.849**
Current model	0.523	0.445	0.568	0.550	0.198	0.271	0.272	**0.404**
With free (spreading)	0.191	0.416	0.218	0.477	0.292	0.271	0.249	**0.302**

*Experimental work is in the column and the theoretical studies are read from the left. The far right column is the average deviation between the theoretical prediction and the experimental result.

Acknowledgments

We thank the industrial sponsors of the University of Maine Paper Surface Science Program. Acknowledgment is made to the donors of The Petroleum Research Fund, administered by the American Chemical Society, for the partial support of this research.

Notation

R^* = dimensionless cylinder radius
R^*_{bulk} = dimensionless radius of spreading drop at center line
R_1 = radius of curvature in the vertical direction
R_2 = radius of curvature perpendicular to vertical
t = time
t^* = dimensionless time
U^* = dimensionless velocity
We = Weber number
ρ = density

Literature Cited

Asai, A., S. Makoto, S. Hirasawa, and T. Okazaki, "Impact of an Ink Drop on Paper," *J. Imag. Sci. Tech.*, **37**, 205 (1993).
Bechtel, S. E., D. B. Bogy, and F. E. Talke, "Impact of a Liquid Drop against a Flat Surface," *IBM J. Res. Dev.*, **25**, 963 (1981).
Chandra, S., and C. T. Avedisian, "On the Collision of a Droplet with a Solid Surface," *Proc. R. Soc. London A*, **432**, 13 (1991).
Cheng, L., "Dynamic Spreading of Drops Impacting onto a Solid Surface," *Ind. Eng. Chem. Process Des. Dev.*, **16**, 192 (1977).
Elliot, T. A., and D. M. Ford, "Dynamic Contact Angles," *Farad. Trans. I.*, **68**, 1814 (1972).
Engel, O. G., "Waterdrop Collisions with Solid Surfaces," *J. Res. Nat. Bur. Stand.*, **54**, 281 (1955).
Field, J. E., M. B. Lesser, and J. P. Dear, "Studies on Two-Dimensional Liquid-Wedge Impact and their Relevance to Liquid-Drop Impact Problems," *Proc. R. Soc. London A*, **401**, 225 (1985).
Greenspan, H. P., "On the Motion of a Small Viscous Droplet that Wets a Surface," *J. Fluid Mech.*, **223**, 57 (1991).
Haley, P. J., and M. J. Miksis, "The Effect of the Contact Line on Droplet Spreading," *J. Fluid Mech.*, **223**, 57 (1991).
Hocking, L. M., and A. D. Rivers, "The Spreading of a Drop by Capillary Action," *J. Fluid Mech.*, **121**, 125 (1982).
Jiang, T. S., S. G. Oh, and J. C. Slattery, "Correlation for Dynamic Contact Angle," *J. Colloid Interf. Sci.*, **69**, 74 (1979).
Lee, S. J., M. M. Denn, M. J. Crochet, and A. B. Metzner, "Compressive Flow between Parallel Disks: 1. Newtonian Fluid with Transverse Viscosity Gradient," *J. Non-Newt. Fluid Mech.*, **10**, 3 (1982).
Lesser, M. B., "Analytic Solutions of Liquid-Drop Impact Problems," *Proc. R. Soc. London A*, **377**, 289 (1981).
Levin, Z., and P. V. Hobbs, "Splashing of Water Drops on Solid and Wetted Surfaces: Hydrodynamics and Charge Separations," *Philos. Trans. R. Soc. London A*, **269**, 555 (1971).
Lopez, J., C. A. Miller, and E. Ruckenstein, "Spreading Kinetics of Liquid Drops on Solids," *J. Colloid Interf. Sci.*, **56**, 460 (1976).
Madejski, J., "Solidification of Droplets on a Cold Surfaces," *Int. J. Heat Mass Trans.*, **19**, 1009 (1976).
Mingheng, S., "Behavior of a Liquid Droplet Impinging on a Solid Surface," *Acta Mech. Sinica*, **17**, 419 (1985).
Mutchler, C. K., and C. L. Larson, "Splash Amounts from Waterdrop Impact on a Smooth Surface," *Water Resour. Res.*, **7**, 195 (1971).
Oliver, J. F., "Initial Stages of Ink Jet Drop Impaction, Spreading and Wetting on Paper," *TAPPI J.*, **67**, 90 (1984).
Schwartz, A. M., and B. T. Silvestre, "Studies of Dynamic Contact Angles on Solids," *J. Colloid Int. Sci.*, **38**, 359 (1972).
Scheller, B. L., "Drop Formation and the Spreading Behavior of Newtonian and Shear-Thinning Liquid Drops Impacting a Solid Surface," PhD Thesis, Univ. of Maine, Orono (1993).
Shi, M. H., T. C. Bai, and J. Yu, "Dynamic Behavior and Heat Transfer of a Liquid Droplet Impinging on a Solid Surface," *Exp. Therm. Fluid Sci.*, **6**, 202 (1993).
Stow, C. D., and M. G. Hadfield, "An Experimental Investigation of Fluid Flow Resulting from the Impact of a Water Drop with an Unyielding Dry Surface," *Proc. R. Soc. London A*, **373**, 419 (1981).
Stow, C. D., and R. D. Stainer, "The Physical Products of a Splashing Water Drop," *J. Meterorol. Soc. Jap.*, **55**, 518 (1977).
Toda, S., *Heat Transfer — Japan. Res.*, **1**(3), 39 (1972).
Trapaga, G., E. F. Matthys, J. J. Valencia, and J. Szekely, "Fluid Flow, Heat Transfer, and Solidification of Molten Metal Droplets Impinging on Substrates: Comparison of Numerical and Experimental Results," *Met. Trans. B.*, **23B**, 701 (1992).
Trapaga, G., and J. Szekely, "Mathematical Modeling of the Isothermal Impingement of Liquid Droplets in Spraying Processes," *Met. Trans. B*, **22B**, 901 (1991).
Wachters, L. H. J., and N. A. J. Weterling, "The Heat Transfer from a Hot Wall to Impinging Water Drops in the Spheroidal State," *Chem. Eng. Sci.*, **21**, 1047 (1986).
Watanabe, T., I. Kuribayashi, T. Honda, and A. Kanzawa, "Deformation and Solidification of a Droplet on a Cold Substrate," *Chem. Eng. Sci.*, **47**, 3059 (1992).
Weast, R. C., *Handbook of Chemistry and Physics*, CRC Press, Cleveland, OH (1975).
Weast, R. C., and M. J. Astle, *CRC Handbook of Data on Organic Compounds*, CRC Press, Boca Raton, FL (1985).
Worthington, A. M., "On the Forms Assumed by Drops of Liquids Falling Vertically on a Horizontal Plate," *Proc. R. Soc. London*, **25**, 261 (1876).
Worthington, A. M., *A Study of Splashes*, Longmans, Green, London (1908).

Manuscript received Feb. 10, 1994, and revision received Aug. 30, 1994.